César Chávez-Olivares, Fernando Reyes-Cortés, Emilio González-Galván

On Explicit Force Regulation with Active Velocity Damping for Robot Manipulators

This paper presents a new interaction control structure that generates a family of explicit force regulators for robot manipulators. The proposed structure includes a term of a class of proportional-type functions in terms of force error; the force error is defined as the difference between a desired force and the actual force measured with a force sensor located at the end-effector. Also, the structure includes a generalized active velocity damping term in order to have a control of the energy dissipation, and a term used to compensate the gravity forces of the links. The stability analysis is performed in Lyapunov sense. An experimental comparison of two new explicit force regulators and the linear proportional structure, on a three degree-of-freedom, direct-drive robot, is presented. Also, proofs of the most important properties of the Cartesian dynamic model, are presented.

Key words: Interaction control, Explicit force control, Direct-drive robot, Lyapunov stability, Cartesian robot control

Eksplicitna regulacija sile robotskog manipulatora aktivnim prigušenjem brzine. Ovaj rad predstavlja novu interakcijsku kontrolnu strukturu koja predstavlja skupinu exsplicitnih regulatora sile za robotske manipulatore. Predložena struktura uključuje član klase funkcija proporcionalnog tipa u smilsu pogreške sile; pogreška sile se definira kao razlika između željene sile i stvarne sile koju mjere senzori postavljeni na kraju manipulatora. Također, struktura uključuje član za generalizirano aktivno prigušenje brzine kako bi se omogućila kontrola disipacije energije i član kojim se kompenzira utjecaj sile gravitacije na članke manipulatora. Analiza stabilnosti je napravljena u smislu Lyapunova. Prikazana je eksperimentalna usporedba dva nova eksplicitna regulatora sile i linearno-proporcionalne strukture na robotu s direktnim pogonom i tri stupnja slobode. Također su prikazani dokazi najvažnijih svojstava kartezijskog dinamičnog modela.

Ključne riječi: Interakcijska kontrola, Eksplicitna regulacija sile, Robot s direktnim pogonom, Stabilnost po Lyapunovu, Kartezijsko upravljanje robotom

1 INTRODUCTION

Applications in which the robotic systems are used, can be classified within two groups in terms of interaction with the environment: if the robot executes tasks where there is no interaction with the environment, then the application belongs to an unconstrained-motion task; if there is interaction, then the application corresponds to a constrained motion task. Force sensing and force control are essential for the successful execution of tasks involving interaction between the manipulator and the environment [1]. Examples of such tasks include pushing, pulling, deburring, scraping, polishing, inserting, mechanical part mating, object contour surface tracking, or assembly. In interaction tasks, the manipulator encounters environmental constraints and the interaction forces are not negligible [2].

As discussed in the next section, different control schemes designed for force control, have been presented in the literature. Among them, the explicit force-control appears in the category of schemes that perform direct force control. The stability of the different explicit force-control schemes, presented in the literature, are studied with linear techniques for transfer functions; the model of the end-effector of the robot in contact with the environment is represented as a linear mechanical system [3]. It is well known that the explicit force control is defined in the context of physical contact. Based on the proportional explicit-force controller scheme, a new control structure for force regulation tasks is presented in this paper. It also includes an active velocity damping term in order to control the energy dissipation. A stability analysis in Lyapunov sense is presented herein, as well as experimental results for three controller schemes. Two of these schemes can be considered as novel contributions of this work.

This paper is organized as follows. Section 2 includes

a review of associated literature. In Section 3, the dynamic model of robot manipulators, its relationship with the Cartesian dynamic model and the principal properties useful in the stability analysis of control schemes, are presented. In Section 4, a new family of explicit force regulators, the stability analysis in Lyapunov sense and case studies of explicit force regulators, are presented. Section 5 describes the experimental platform used to gather evidence of the performance of the study cases. Finally, conclusions are presented in Section 6. In the Appendix, we present an alternative proof of the main properties of the Cartesian dynamic model, which are widely used in Cartesian robot control.

2   LITERATURE REVIEW

During the last three decades, many researchers have worked on new schemes of active interaction control of robot manipulators. As a result, different control schemes have been proposed in the literature, as surveyed by Whitney [4], De Schutter et. al [5], and Chiaverini et. al [6]. Interaction control strategies can be grouped within two categories [7]: those performing indirect force control and those performing direct force control. The main difference between the two categories is that indirect methods achieve force control via motion control without imposing a force set-point; direct methods, however, offer the possibility of controlling the contact force to a desired value. Among the most important indirect interaction control approaches are stiffness control [8–12] and impedance control [1, 2, 13–15]. While, among the main direct interaction control approaches, we can consider the explicit force control [16–18], the hybrid force/position control [19–23] and the parallel force/motion control [24, 25].

The explicit force control approach has been implemented in different ways [16]. This scheme enables the control of the contact force to a desired value. The torques applied by the robot joints are commanded as a result of a function of the force error, where the force error is defined as the difference between the reference force and the actual interaction force measured with a force/torque sensor. The most relevant schemes in which the explicit force control is implemented are: proportional control, integral control, proportional-integral control, and proportional-derivative control [1, 18]. In [26], a proportional-integral scheme has been implemented on a robot applied to rehabilitation.

In the approach referred to as hybrid force/position control [19], the workspace of the robot is divided into orthogonal directions that are constrained either in force or position, and an appropriate force or position controller for each direction is designed. This approach is aimed at controlling the position along the unconstrained task directions and force along the constrained task directions. In

order to implement this interaction control strategy, a detailed model of the environment is required.

The parallel force/motion control is an interaction control strategy that enables simultaneous movement control and force control [24]. The main idea is the use of an inner position-control loop that works in parallel with a force-control loop. Conflicting situations between the position and force tasks are managed by using a priority strategy: the force-control loop is designed to prevail over the position-control loop. Recent works include observers in order to have an estimation of velocity and also to increase the performance of the system [25].

The stiffness control proposed by Salisbury [8], is an interaction control approach designed to achieve a desired static behavior of the interaction of a robot manipulator with the environment [2]. In this form, it is essentially a Cartesian proportional-derivative (PD) position controller, with position and velocity feedback gains adjusted in order to obtain different apparent impedances. The stiffness control has been implemented in different ways. Among them, an approach based on variable stiffness, referred to as self-controlled stiffness function, is used for unknown environments [9]; in reference [10], an approach based on adaptive stiffness characteristics for interaction with unknown environments, is presented; in [12], new sufficient stability conditions for stiffness control based on a Lyapunov-Hamiltonian function, are presented. In this case, stiffness control is used for robot-aided rehabilitation.

The approach referred to as impedance control was introduced by Hogan [2]; it is based on the control of the relationship between the interaction force and positioning errors resulting from this force. The dynamic interaction between the manipulator and its environment can be regulated and controlled by changing its mechanical impedance. The strategy introduced by Hogan, presents a general and unified approach to implement, in a robot manipulator, an impedance controller and generate a linear mass-spring-damper, closed-loop system. Based on this approach, several control schemes have been developed for interaction control. Among them, a robust nonlinear impedance control [13]; the hybrid impedance control (HIC) [27], which is a combination of impedance control and the hybrid position/force control; an adaptive impedance control approach, which considers parametric uncertainties in the robot model [28]; an adaptive version of HIC [29] is used in order to take into account the parametric uncertainties in the robot model. Recent control schemes based on inverse-dynamics for dynamic compensation [15], yielding a control structure in terms of proportional-derivative-like functions of the impedance error [14], have been developed. These structures were designed with the purpose of being useful both for unconstrained and constrained motion. Further-

more, these schemes have been tested on a two-degree-of-freedom, direct-drive robot, and present better performance than Hogan's impedance approach, both on path-following tasks in unconstrained motion and in the case of tasks in which interaction with the environment occurs.

3 DYNAMIC MODEL OF ROBOT MANIPULATORS

The dynamic analysis of the robot arm determines a relationship between the joint torques/forces applied by the actuators and the motion of the robot. The robot dynamics in joint space with rigid links is described by the joint positions, velocities and accelerations as functions of time. The dynamic model is given by

$$\boldsymbol{\tau} \;=\; M(\boldsymbol{q})\ddot{\boldsymbol{q}} + C(\boldsymbol{q},\dot{\boldsymbol{q}})\dot{\boldsymbol{q}} + \boldsymbol{g}(\boldsymbol{q}) + \boldsymbol{f}(\dot{\boldsymbol{q}}) \qquad (1)$$

where $\boldsymbol{q} \in \mathbb{R}^n$ is the vector of joint displacements, $\dot{\boldsymbol{q}} \in \mathbb{R}^n$ is the vector of joint velocities, $\ddot{\boldsymbol{q}} \in \mathbb{R}^n$ is the vector of joint accelerations, $\boldsymbol{\tau} \in \mathbb{R}^n$ is the vector of applied generalized forces/torques, $M(\boldsymbol{q}) \in \mathbb{R}^{n\times n}$ is the symmetric positive definite manipulator inertia matrix, $C(\boldsymbol{q},\dot{\boldsymbol{q}}) \in \mathbb{R}^{n\times n}$ is the matrix of centripetal and Coriolis torques, $\boldsymbol{g}(\boldsymbol{q}) \in \mathbb{R}^n$ is the vector of gravitational torques obtained as the gradient of the robot total potential energy $\mathcal{U}(\boldsymbol{q})$. $\boldsymbol{f}(\dot{\boldsymbol{q}}) \in \mathbb{R}^n$ is the friction torque vector. In this paper we consider the common viscous-friction model.

The dynamic model of robot manipulators (1) can be expressed in Cartesian-space by using a coordinate change. Is it necessary to consider the relationship between joint velocities and the end-effector Cartesian velocities $\dot{\boldsymbol{x}} = J(\boldsymbol{q})\dot{\boldsymbol{q}}$, where $J(\boldsymbol{q})$ is referred to as the Jacobian matrix.

A few properties related to Cartesian model can be mentioned as follows [30]:

Property 1. A relationship exists between the applied forces $\boldsymbol{f}_\chi$ in Cartesian-space at the end effector, and the applied torques $\boldsymbol{\tau}$ on the joints. This relationship is known as the Jacobian Transposed Controller [31], and it is given by,

$$\boldsymbol{\tau} \;=\; J^T(\boldsymbol{q})\boldsymbol{f}_\chi \qquad (2)$$

where

$$\boldsymbol{f}_\chi - \boldsymbol{f}_e \;=\; M_\chi \ddot{\boldsymbol{x}} + C_\chi \dot{\boldsymbol{x}} + \boldsymbol{g}_\chi + \boldsymbol{f}_{f\chi} \qquad (3)$$

Equation (3) is referred to as the Cartesian dynamic model, the term $\boldsymbol{f}_e$ has been included in order to consider the external forces applied to the end-effector, such as the forces produced during an interaction task. The terms of the Cartesian dynamic model can be described in terms of the joint-space dynamic model and the Jacobian matrix, by considering the following properties.

Property 2. Matrix M_χ is described in terms of matrices $J(\boldsymbol{q})$ and $M(\boldsymbol{q})$ as follows,

$$M_\chi \;=\; J^{-T}(\boldsymbol{q})M(\boldsymbol{q})J^{-1}(\boldsymbol{q}) \qquad (4)$$

Property 3. Matrix C_χ is described in terms of the matrices $J(\boldsymbol{q})$, $C(\boldsymbol{q},\dot{\boldsymbol{q}})$ and M_χ as,

$$\begin{aligned} C_\chi \;=\;\; & J^{-T}(\boldsymbol{q})C(\boldsymbol{q},\dot{\boldsymbol{q}})J^{-1}(\boldsymbol{q}) \\ & -M_\chi \dot{J}(\boldsymbol{q})J^{-1}(\boldsymbol{q}) \end{aligned} \qquad (5)$$

where $\dot{J}(\boldsymbol{q}) = \partial J(\boldsymbol{q})/\partial t$.

Property 4. Matrix $\boldsymbol{g}_\chi$ is described in terms of matrix $J(\boldsymbol{q})$ and vector $\boldsymbol{g}(\boldsymbol{q})$ as,

$$\boldsymbol{g}_\chi \;=\; J^{-T}(\boldsymbol{q})\boldsymbol{g}(\boldsymbol{q}) \qquad (6)$$

Property 5. Matrix $\boldsymbol{f}_{f\chi}$ is described in terms of matrix $J(\boldsymbol{q})$ and vector $\boldsymbol{f}(\dot{\boldsymbol{q}})$ as follows,

$$\boldsymbol{f}_{f\chi} \;=\; J^{-T}(\boldsymbol{q})\boldsymbol{f}(\dot{\boldsymbol{q}}) \qquad (7)$$

Property 6. Matrix M_χ is symmetric and definite positive,

$$M_\chi > 0, \qquad M_\chi = M_\chi^T \qquad (8)$$

Property 7. Matrix M_χ is upper and lower bounded by,

$$\lambda_{\min}\{M_\chi\}\, I \leq M_\chi \leq \lambda_{\max}\{M_\chi\}\, I \qquad (9)$$

Property 8. Since $\dot{M}_\chi = C_\chi + C_\chi^T$, matrix $\dot{M}_\chi - 2C_\chi$ is skew-symmetric, that is,

$$\frac{1}{2}\dot{\boldsymbol{x}}^T\left[\dot{M}_\chi - 2C_\chi\right]\dot{\boldsymbol{x}} \equiv 0 \qquad (10)$$

Once the principal properties and the relationship between Cartesian-space and joint-space dynamic models are presented, it is possible to define a control problem and a solution proposal, as presented in the following sections.

4 A NEW FAMILY OF EXPLICIT FORCE REGULATORS WITH ACTIVE VELOCITY DAMPING

In the case of constrained-motion applications, it is very important to have a control of the interaction forces in order to achieve a successful maneuver execution. [1]. In this case, the manipulator encounters environmental constraints and the interaction forces are not negligible [2]. If a sensor force is available, then it is possible to create control structures in which the applied torques to the robot are commanded as a function of force error $\tilde{\boldsymbol{f}}$, defined as the

difference between a desired force $\boldsymbol{f}_d$ and the actual inter-action force $\boldsymbol{f}(t)$, which is measured with the force sensor. The objective of this control scheme is to have a direct control of the forces applied by the end-effector of the manipulator, over the environment. This control scheme is referred to as explicit force-control approach and has been implemented in many ways, such as the proportional control, integral control, proportional-integral control, and the proportional-derivative control. In this section, a new family of explicit force regulators based on the proportional structure, is presented.

4.1   Control Problem Statement

In this paper, an *explicit force-regulator approach* will be given a Cartesian robot-control structure. Such an approach enables the control of a force applied to the environment; the desired force is constant, which means that the objective of the explicit force-regulator is to apply the desired constant force to the environment, at all times. This feature serves as a justification of the term *regulation* as a desired force that varies over time, is not considered in this scheme.

In formal terms, the control objective consists on finding $\boldsymbol{f}_\chi$ such that

$$\lim_{t \to \infty} \boldsymbol{f}(t) = \boldsymbol{f}_d \tag{11}$$

where $\boldsymbol{f}_d \in \mathbb{R}^n$ is a given constant vector which represents the desired forces applied to environment.

With the purpose of evaluating if the controller achieves the control objective, the asymptotic stability of the origin of the closed-loop system, in the sense of Lyapunov, is studied. With this purpose, the position control objective is rewritten as,

$$\lim_{t \to \infty} \tilde{\boldsymbol{f}}(t) = \boldsymbol{0} \tag{12}$$

where $\tilde{\boldsymbol{f}} \in \mathbb{R}^n$ represents the force-error vector applied to environment or simply, force error, which is defined by

$$\tilde{\boldsymbol{f}} = \boldsymbol{f}_d - \boldsymbol{f}(t) \tag{13}$$

4.2   Proposition

In order to achieve the control objective given by (12) and to satisfy our definition of explicit force-regulator approach, a new structure of controllers is proposed as,

$$\begin{aligned} \boldsymbol{f}_\chi &= \nabla \mathcal{U}_a \left(K_{pf}, \tilde{\boldsymbol{f}} \right) - \boldsymbol{f}_v \left(K_v, \dot{\boldsymbol{x}} \right) \\ &\quad + \boldsymbol{g}_\chi + \boldsymbol{f}_e \end{aligned} \tag{14}$$

The first term corresponds to a proportional-type function of force error designed as $\nabla \mathcal{U}_a \left(K_{pf}, \tilde{\boldsymbol{f}} \right) = \boldsymbol{0}$ when

$\tilde{\boldsymbol{f}} = 0$. The second term is a generalized, active velocity-damping term, used with the objective of manipulating the energy dissipation, where K_v is referred to as gain damping matrix; this term is designed as $\dot{\boldsymbol{x}} \boldsymbol{f}_v \left(K_v, \dot{\boldsymbol{x}} \right) > 0$ for $\dot{\boldsymbol{x}} \neq \boldsymbol{0}$ and $\boldsymbol{f}_v \left(K_v, \dot{\boldsymbol{x}} \right) = \boldsymbol{0}$ for $\dot{\boldsymbol{x}} = \boldsymbol{0}$. The third term represents the gravity forces. It is important to notice that a partial knowledge of the dynamic model of the manipulator is needed, i.e., in order to compute $\boldsymbol{g}_\chi$, the vector of gravity torques $\boldsymbol{g}(\boldsymbol{q})$, is required.

In order to analyze the closed-loop system, a consideration of a model used for the representation of the environment, is needed. In robotics literature, the stiffness model is commonly used for the representation of the environment. It is given by,

$$\boldsymbol{f}_e = K_e(\boldsymbol{x} - \boldsymbol{x}_e) \tag{15}$$

where K_e is referred to as the environment's stiffness-matrix, the term $\boldsymbol{x}_e$ denotes a constant position where the environment is located, while $\boldsymbol{x}$ denotes the actual position of the end-effector.

Taking into account that the measured force is represented by $\boldsymbol{f}(t)$, when the end-effector is in contact with the environment it becomes $\boldsymbol{f}(t) = \boldsymbol{f}_e$; then, in terms of the state vector $\begin{bmatrix} \tilde{\boldsymbol{f}}^T & \dot{\boldsymbol{x}}^T \end{bmatrix}^T \in \mathbb{R}^{2n}$, the equation that describes the closed loop system is obtained by combining equations (3) and (14) and, assuming that $\boldsymbol{f}_d$ is a constant vector, we obtain

$$\frac{d}{dt} \begin{bmatrix} \tilde{\boldsymbol{f}} \\ \dot{\boldsymbol{x}} \end{bmatrix} =$$

$$\begin{bmatrix} -K_e \dot{\boldsymbol{x}} \\ M_\chi^{-1} \left[\nabla \mathcal{U}_a \left(K_{pf}, \tilde{\boldsymbol{f}} \right) - \boldsymbol{f}_v \left(K_v, \dot{\boldsymbol{x}} \right) \\ -C_\chi \dot{\boldsymbol{x}} - \boldsymbol{f}_{f\chi} \right] \end{bmatrix} \tag{16}$$

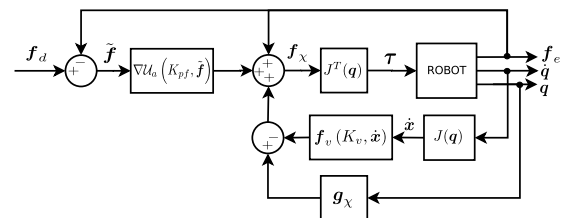Figure 1 shows a block diagram of the control scheme.

Fig. 1.   *Block diagram of the proposed control scheme*

4.3   Stability proof in Lyapunov sense

The equilibrium point of the system (16) exists under the following conditions

(a) A singularity-free work space, i.e., $\text{rank}[J(\boldsymbol{q})] = n$, is considered

(b) Since $M_\chi > 0 \Rightarrow \exists\, M_\chi^{-1} > 0$, then

$$
\begin{aligned}
\nabla \mathcal{U}_a \left(K_{pf}, \tilde{\boldsymbol{f}} \right) &= \boldsymbol{0} \Longleftrightarrow \tilde{\boldsymbol{f}} = \boldsymbol{0}, K_{pf} > \boldsymbol{0} \\
\boldsymbol{f}_v \left(K_v, \dot{\boldsymbol{x}} \right) &= \boldsymbol{0} \Longleftrightarrow \dot{\boldsymbol{x}} = \boldsymbol{0}, K_v > \boldsymbol{0} \\
C_\chi \dot{\boldsymbol{x}} &= \boldsymbol{0} \Longleftrightarrow \dot{\boldsymbol{x}} = \boldsymbol{0} \\
\boldsymbol{f}_{f\chi} &= \boldsymbol{0} \Longleftrightarrow \dot{\boldsymbol{x}} = \boldsymbol{0}
\end{aligned}
$$

In order to carry out the stability analysis of the dynamic system given in (16), and before a candidate Lyapunov-like function is presented, it is important to introduce a function that will be included within the candidate Lyapunov function. According to the environment's stiffness model, the stiffness matrix has the property of being diagonal and positive definite: $K_e = K_e^T > 0$ then $K_e^{-1} > 0$ exists. Consider the following scalar, positive definite function,

$$
\mathcal{U}\left(K_e^{-1}, K_{pf}, \tilde{\boldsymbol{f}} \right) =
$$

$$
\begin{bmatrix} \sqrt{\mathcal{U}_1 \left(K_{pf1}, \tilde{f}_1 \right)} \\ \vdots \\ \sqrt{\mathcal{U}_n \left(K_{pfn}, \tilde{f}_n \right)} \end{bmatrix}^T K_e^{-1} \begin{bmatrix} \sqrt{\mathcal{U}_1 \left(K_{pf1}, \tilde{f}_1 \right)} \\ \vdots \\ \sqrt{\mathcal{U}_n \left(K_{pfn}, \tilde{f}_n \right)} \end{bmatrix} \quad (17)
$$

and the derivative with respect to time is given by,

$$
\frac{d}{dt} \mathcal{U} \left(K_e^{-1}, K_{pf}, \tilde{\boldsymbol{f}} \right) = \dot{\tilde{\boldsymbol{f}}}^T K_e^{-1} \nabla \mathcal{U} \quad (18)
$$

for convenience, the above function is rewritten in the following form,

$$
\frac{d}{dt} \mathcal{U} \left(K_e^{-1}, K_{pf}, \tilde{\boldsymbol{f}} \right) = \dot{\tilde{\boldsymbol{f}}}^T K_e^{-1} \nabla \mathcal{U}_a \left(K_{pf}, \tilde{\boldsymbol{f}} \right) \quad (19)
$$

Now, consider the following candidate Lyapunov function,

$$
V(\dot{\boldsymbol{x}}, \tilde{\boldsymbol{f}}) = \frac{1}{2} \dot{\boldsymbol{x}}^T M_\chi \dot{\boldsymbol{x}} + \mathcal{U} \left(K_e^{-1}, K_{pf}, \tilde{\boldsymbol{f}} \right) \quad (20)
$$

where the first term is positive definite due to its quadratic form, while a positive definite and radially unbounded function $\mathcal{U}\left(K_e^{-1}, K_{pf}, \tilde{\boldsymbol{f}} \right)$ is chosen, in order to keep the same properties on the function $V(\dot{\boldsymbol{x}}, \tilde{\boldsymbol{f}})$.

The total derivative of the candidate Lyapunov function (20), with respect to time, is,

$$
\begin{aligned}
\dot{V}(\dot{\boldsymbol{x}}, \tilde{\boldsymbol{f}}) = {}& \dot{\boldsymbol{x}}^T M_\chi \ddot{\boldsymbol{x}} + \frac{1}{2} \dot{\boldsymbol{x}}^T \dot{M}_\chi \dot{\boldsymbol{x}} \\
& + \dot{\tilde{\boldsymbol{f}}}^T K_e^{-1} \nabla \mathcal{U}_a \left(K_{pf}, \tilde{\boldsymbol{f}} \right) \quad (21)
\end{aligned}
$$

By substituting $\dot{\tilde{\boldsymbol{f}}} = -K_e \dot{\boldsymbol{x}}$ and $M_\chi \ddot{\boldsymbol{x}} = \nabla \mathcal{U}_a \left(K_{pf}, \tilde{\boldsymbol{f}} \right) - \boldsymbol{f}_v \left(K_v, \dot{\boldsymbol{x}} \right) - C_\chi \dot{\boldsymbol{x}} - \boldsymbol{f}_{f\chi}$ from the closed-loop equation (16), and considering that $\dot{\boldsymbol{x}}^T \left[\frac{1}{2} \dot{M}_\chi - C_\chi \right] \dot{\boldsymbol{x}} = 0$, we get

$$
\begin{aligned}
\dot{V}(\dot{\boldsymbol{x}}, \tilde{\boldsymbol{f}}) = {}& \dot{\boldsymbol{x}}^T \nabla \mathcal{U}_a \left(K_{pf}, \tilde{\boldsymbol{f}} \right) - \dot{\boldsymbol{x}}^T \boldsymbol{f}_v \left(K_v, \dot{\boldsymbol{x}} \right) \\
& - \dot{\boldsymbol{x}}^T C_\chi \dot{\boldsymbol{x}} - \dot{\boldsymbol{x}}^T \boldsymbol{f}_{f\chi} + \frac{1}{2} \dot{\boldsymbol{x}}^T \dot{M}_\chi \dot{\boldsymbol{x}} \\
& - \dot{\boldsymbol{x}}^T K_e K_e^{-1} \nabla \mathcal{U}_a \left(K_{pf}, \tilde{\boldsymbol{f}} \right) \\
= {}& -\dot{\boldsymbol{x}}^T \boldsymbol{f}_v \left(K_v, \dot{\boldsymbol{x}} \right) - \dot{\boldsymbol{x}}^T \boldsymbol{f}_{f\chi} \leq 0 \quad (22)
\end{aligned}
$$

where $\dot{\boldsymbol{x}}^T \boldsymbol{f}_v \left(K_v, \dot{\boldsymbol{x}} \right) > 0$ and $\dot{\boldsymbol{x}}^T \boldsymbol{f}_{f\chi} > 0$ due to $\boldsymbol{f}_{f\chi} = B_\chi \dot{\boldsymbol{x}}$, from the viscous friction model $B_\chi = J^{-T} B J^{-1}$. Since $\dot{V}(\dot{\boldsymbol{x}}, \tilde{\boldsymbol{f}})$ is a negative semidefinite function, in agreement with Lyapunov's direct method, the control law yields a stable closed loop system.

Since the closed-loop equation (16) is independent of time explicitly, the use of La Salle's theorem [32] is a valid way to analyze the asymptotic stability of the origin. With this purpose, the set Ω is used:

$$
\begin{aligned}
\Omega &= \left\{ \boldsymbol{\omega} \in \mathbb{R}^{2n} : \dot{V}(\omega) = 0 \right\} \\
&= \left\{ \boldsymbol{\omega} = \begin{bmatrix} \tilde{\boldsymbol{f}} \\ \dot{\boldsymbol{x}} \end{bmatrix} \in \mathbb{R}^{2n} : \dot{V}(\dot{\boldsymbol{x}}, \tilde{\boldsymbol{f}}) = 0 \right\} \\
&= \left\{ \tilde{\boldsymbol{f}} \in \mathbb{R}^n, \dot{\boldsymbol{x}} = \boldsymbol{0} \in \mathbb{R}^n \right\} \quad (23)
\end{aligned}
$$

Observe that $\dot{V}(\dot{\boldsymbol{x}}, \tilde{\boldsymbol{f}}) = 0$ if and only if $\dot{\boldsymbol{x}} = \boldsymbol{0}$. For a solution $\boldsymbol{\omega}(t)$ to belong to Ω for all $t \geq 0$, it is necessary and sufficient that $\dot{\boldsymbol{x}}(t) = \boldsymbol{0}$ for all $t \geq 0$. Therefore, it must also hold that $\ddot{\boldsymbol{x}}(t) = \boldsymbol{0}$ for all $t \geq 0$. Taking this into account we conclude, from the closed-loop equation (16), that if $\omega(t) \in \Omega$ for all $t \geq 0$ then

$$
\boldsymbol{0} = M_\chi^{-1} \nabla \mathcal{U}_a \left(K_{pf}, \tilde{\boldsymbol{f}} \right) \quad (24)
$$

which means that $\tilde{\boldsymbol{f}} = \boldsymbol{0}$ for all $t \geq 0$. Thus, $\left[\tilde{\boldsymbol{f}}(0)^T \quad \dot{\boldsymbol{x}}(0)^T \right]^T = \boldsymbol{0} \in \mathbb{R}^{2n}$ is the only initial condition in Ω for which $\boldsymbol{\omega}(t) \in \Omega$ for all $t \geq 0$. Then, according to La Salle's theorem, this is enough to guarantee asymptotic stability of the origin $\left[\tilde{\boldsymbol{f}}^T \quad \dot{\boldsymbol{x}}^T \right]^T = \boldsymbol{0} \in \mathbb{R}^{2n}$.

As a result,

$$
\begin{aligned}
\lim_{t \to \infty} \tilde{\boldsymbol{f}}(t) &= \boldsymbol{0} \\
\lim_{t \to \infty} \dot{\boldsymbol{x}}(t) &= \boldsymbol{0}
\end{aligned}
$$

that is, the control objective is achieved.

4.4 Study cases

Several controllers can be generated by using the proposed structure (14); some examples are,

(i) Linear proportional force-regulation scheme with linear active velocity-damping

The linear proportional force regulator [16] belongs to the family of explicit force regulators given in (14). The structure of this regulator is given by

$$\boldsymbol{f}_\chi = K_{pf}\tilde{\boldsymbol{f}} - K_v\dot{\boldsymbol{x}} + \boldsymbol{g}_\chi + \boldsymbol{f}_e \qquad (25)$$

In order to carry out the stability analysis of the dynamic system given in (16) for this controller, the following candidate Lyapunov function is used,

$$V(\dot{\boldsymbol{x}}, \tilde{\boldsymbol{f}}) = \frac{1}{2}\dot{\boldsymbol{x}}^T M_\chi \dot{\boldsymbol{x}}$$
$$+ \frac{1}{2}\begin{bmatrix} \sqrt{K_{pf1}\tilde{f}_1^2} \\ \vdots \\ \sqrt{K_{pfn}\tilde{f}_n^2} \end{bmatrix}^T K_e^{-1} \begin{bmatrix} \sqrt{K_{pf1}\tilde{f}_1^2} \\ \vdots \\ \sqrt{K_{pfn}\tilde{f}_n^2} \end{bmatrix} \qquad (26)$$

Furthermore, the total derivative of the candidate Lyapunov function (26), with respect to time, is

$$\begin{aligned} \dot{V}(\dot{\boldsymbol{x}}, \tilde{\boldsymbol{f}}) &= \dot{\boldsymbol{x}}^T K_{pf}\tilde{\boldsymbol{f}} - \dot{\boldsymbol{x}}^T K_v\dot{\boldsymbol{x}} - \dot{\boldsymbol{x}}^T C_\chi\dot{\boldsymbol{x}} - \dot{\boldsymbol{x}}^T \boldsymbol{f}_{f\chi} \\ &\quad + \frac{1}{2}\dot{\boldsymbol{x}}^T \dot{M}_\chi\dot{\boldsymbol{x}} - \dot{\boldsymbol{x}}^T K_e K_e^{-1} K_{pf}\tilde{\boldsymbol{f}} \\ &= -\dot{\boldsymbol{x}}^T K_v\dot{\boldsymbol{x}} - \dot{\boldsymbol{x}}^T \boldsymbol{f}_{f\chi} \le 0 \qquad (27) \end{aligned}$$

(ii) Atan proportional force regulation scheme with atan active velocity damping

The atan proportional force regulator scheme is a new structure that does not appear in the force-control literature, which is given by

$$\boldsymbol{f}_\chi = K_{pf}\,\mathbf{atan}(\tilde{\boldsymbol{f}}) - K_v\,\mathbf{atan}(\dot{\boldsymbol{x}}) + \boldsymbol{g}_\chi + \boldsymbol{f}_e \qquad (28)$$

where the following, simplified notation, is used,

$$\mathbf{atan}(\boldsymbol{\alpha}) = \begin{bmatrix} \text{atan}(\alpha_1) \\ \vdots \\ \text{atan}(\alpha_n) \end{bmatrix} \qquad (29)$$

for $\boldsymbol{\alpha} = \tilde{\boldsymbol{f}}, \dot{\boldsymbol{x}}$

Furthermore, the stability analysis can be carried out by selecting the following candidate Lyapunov function,

$$V(\dot{\boldsymbol{x}}, \tilde{\boldsymbol{f}}) = \frac{1}{2}\dot{\boldsymbol{x}}^T M_\chi \dot{\boldsymbol{x}} + \boldsymbol{v}^T K_e^{-1}\boldsymbol{v} \qquad (30)$$

where

$$\boldsymbol{v} = \begin{bmatrix} \sqrt{K_{pf1}\left(\tilde{f}_1\text{atan}\left(\tilde{f}_1\right) - \frac{1}{2}\ln\left(1 + \tilde{f}_1^2\right)\right)} \\ \vdots \\ \sqrt{K_{pfn}\left(\tilde{f}_n\text{atan}\left(\tilde{f}_n\right) - \frac{1}{2}\ln\left(1 + \tilde{f}_n^2\right)\right)} \end{bmatrix}$$

The total derivative of the candidate Lyapunov function (30), with respect to time, is

$$\begin{aligned} \dot{V}(\dot{\boldsymbol{x}}, \tilde{\boldsymbol{f}}) &= \dot{\boldsymbol{x}}^T K_{pf}\,\mathbf{atan}(\tilde{\boldsymbol{f}}) - \dot{\boldsymbol{x}}^T K_v\,\mathbf{atan}(\dot{\boldsymbol{x}}) \\ &\quad - \dot{\boldsymbol{x}}^T C_\chi\dot{\boldsymbol{x}} - \dot{\boldsymbol{x}}^T \boldsymbol{f}_{f\chi} + \frac{1}{2}\dot{\boldsymbol{x}}^T \dot{M}_\chi\dot{\boldsymbol{x}} \\ &\quad - \dot{\boldsymbol{x}}^T K_e K_e^{-1} K_{pf}\,\mathbf{atan}(\tilde{\boldsymbol{f}}) \\ &= -\dot{\boldsymbol{x}}^T K_v\,\mathbf{atan}(\dot{\boldsymbol{x}}) - \dot{\boldsymbol{x}}^T \boldsymbol{f}_{f\chi} \le 0 \quad (31) \end{aligned}$$

(iii) RSR proportional force regulation scheme with RSR active velocity damping

The Reciprocal Square-Root (RSR) type force regulator, is a new structure that has not been referenced in the force-control literature, whose model is given by

$$\boldsymbol{f}_\chi = K_{pf}\frac{\tilde{\boldsymbol{f}}}{\sqrt{1 + \tilde{\boldsymbol{f}}^2}} - K_v\frac{\dot{\boldsymbol{x}}}{\sqrt{1 + \dot{\boldsymbol{x}}^2}} + \boldsymbol{g}_\chi + \boldsymbol{f}_e \quad (32)$$

where, by using a simplified notation, the following vectorial function is described,

$$\frac{\boldsymbol{\alpha}}{\sqrt{1 + \boldsymbol{\alpha}^2}} = \begin{bmatrix} \frac{\alpha_1}{\sqrt{1+\alpha_1^2}} \\ \vdots \\ \frac{\alpha_n}{\sqrt{1+\alpha_n^2}} \end{bmatrix} \qquad (33)$$

for $\boldsymbol{\alpha} = \tilde{\boldsymbol{f}}, \dot{\boldsymbol{x}}$

The following candidate Lyapunov function is used,

$$V(\dot{\boldsymbol{x}}, \tilde{\boldsymbol{f}}) = \frac{1}{2}\dot{\boldsymbol{x}}^T M_\chi \dot{\boldsymbol{x}}$$
$$+ \begin{bmatrix} \sqrt{K_{pf1}\sqrt{1 + \tilde{f}_1^2}} \\ \vdots \\ \sqrt{K_{pfn}\sqrt{1 + \tilde{f}_n^2}} \end{bmatrix}^T K_e^{-1} \begin{bmatrix} \sqrt{K_{pf1}\sqrt{1 + \tilde{f}_1^2}} \\ \vdots \\ \sqrt{K_{pfn}\sqrt{1 + \tilde{f}_n^2}} \end{bmatrix}$$
$$(34)$$

The total derivative of the candidate Lyapunov function (34), with respect to time, is

$$
\begin{aligned}
\dot{V}(\dot{\boldsymbol{x}}, \tilde{\boldsymbol{f}}) & = & \dot{\boldsymbol{x}}^T K_{pf} \frac{\tilde{\boldsymbol{f}}}{\sqrt{1 + \tilde{\boldsymbol{f}}^2}} - \dot{\boldsymbol{x}}^T K_v \frac{\dot{\boldsymbol{x}}}{\sqrt{1 + \dot{\boldsymbol{x}}^2}} \\
& & -\dot{\boldsymbol{x}}^T C_\chi \dot{\boldsymbol{x}} - \dot{\boldsymbol{x}}^T \boldsymbol{f}_{f\chi} + \frac{1}{2} \dot{\boldsymbol{x}}^T \dot{M}_\chi \dot{\boldsymbol{x}} \\
& & -\dot{\boldsymbol{x}}^T K_e K_e^{-1} K_{pf} \frac{\tilde{\boldsymbol{f}}}{\sqrt{1 + \tilde{\boldsymbol{f}}^2}} \\
& = & -\dot{\boldsymbol{x}}^T K_v \frac{\dot{\boldsymbol{x}}}{\sqrt{1 + \dot{\boldsymbol{x}}^2}} - \dot{\boldsymbol{x}}^T \boldsymbol{f}_{f\chi} \leq 0 \quad (35)
\end{aligned}
$$

For all the proposed controllers, in order to obtain asymptotic stability, we apply LaSalle's theorem in the region

$$
\Omega = \left\{ \begin{bmatrix} \tilde{\boldsymbol{f}} \\ \dot{\boldsymbol{x}} \end{bmatrix} \in \mathbb{R}^{2n} : \dot{V}(\dot{\boldsymbol{x}}, \tilde{\boldsymbol{f}}) = 0 \right\} \quad (36)
$$

the unique invariant is $\begin{bmatrix} \tilde{\boldsymbol{f}}^T & \dot{\boldsymbol{x}}^T \end{bmatrix}^T = 0 \in \mathbb{R}^{2n}$.

In the next section, the experimental results for the aforementioned controllers, implemented on a three-degree-of-freedom direct-drive robot, are presented.

5 EXPERIMENTAL RESULTS

Experimental results, obtained by using an anthropomorphic direct-drive robot which was designed and built at the Robotics laboratory of Benemérita Universidad Autónoma de Puebla (BUAP), are presented. The three-degree-of-freedom robot "Rotradi", consists of three 6061 aluminum links, actuated by brushless direct-drive servo actuators used to drive the joints without gear reduction. The motors used in "Rotradi" are DM-1050A, DM-1150A and DM-1015B models from Parker Compumotor, for the base, the shoulder and elbow joints, respectively. The servos are operated in torque mode, which means that the motor acts as a torque source and they accept an analog voltage as a reference of torque signal. The servo-actuators features are shown in Table 1. The robot system has a device designed for reading the encoders and generate reference voltages, which is a motion control board from Precision MicroDynamics Inc. The control algorithms are written in C code and run in real time with a 2.5 ms sample period on a Pentium-1 computer at 166 MHz.

In order to perform the force sensing, a six-axis force/torque sensor ATI FT Gamma SI-130-10 with force range of ± 130 N and torque range of ± 10 Nm, is mounted at the end-effector of the robot manipulator. The sensor is connected to a 3.6 GHz Pentium-IV computer, and the signals are processed by using a Visual C++ application.
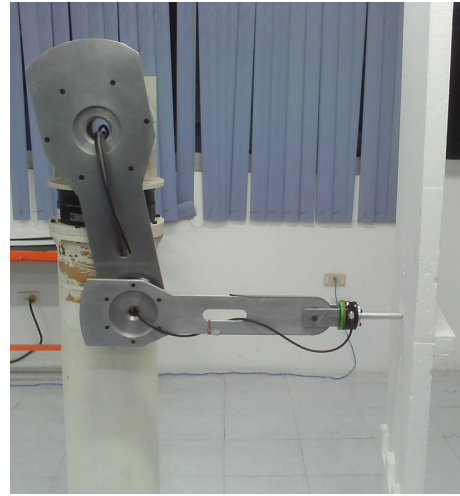

Fig. 2. Experimental robot "Rotradi"

The communication between the robot manipulator and the force sensor was enabled by a communication protocol based on interruption signals sent via parallel port.

The gravitational-torques vector for our experimental manipulator is taken from [33], it is given by,

$$
\begin{aligned}
g_1(\boldsymbol{q}) & = & 0 \\
g_2(\boldsymbol{q}) & = & 55.628 \sin(q_2) - 0.272 \cos(q_2) \\
& & +1.996 \sin(q_2 + q_3) + 0.695 \cos(q_2 + q_3) \\
g_3(\boldsymbol{q}) & = & 1.996 \sin(q_2 + q_3) + 0.695 \cos(q_2 + q_3)
\end{aligned}
$$

while the elements of the Jacobian matrix are given as follows,

$$
\begin{aligned}
J_{1,1} & = & -0.25 \sin(q_1) \\
& & -\cos(q_1) [0.45 \sin(q_2) + 0.69 \sin(q_2 + q_3)] \\
J_{1,2} & = & -\sin(q_1) [0.45 \cos(q_2) + 0.69 \cos(q_2 + q_3)] \\
J_{1,3} & = & -0.69 \sin(q_1) \cos(q_2 + q_3) \\
J_{2,1} & = & 0.25 \cos(q_1) \\
& & -\sin(q_1) [0.45 \sin(q_2) + 0.69 \sin(q_2 + q_3)] \\
J_{2,2} & = & \cos(q_1) [0.45 \cos(q_2) + 0.69 \cos(q_2 + q_3)] \\
J_{2,3} & = & 0.69 \cos(q_1) \cos(q_2 + q_3) \\
J_{3,1} & = & 0 \\
J_{3,2} & = & 0.45 \sin(q_2) + 0.69 \sin(q_2 + q_3) \\
J_{3,3} & = & 0.69 \sin(q_2 + q_3)
\end{aligned}
$$

Figure 3 shows the auxiliary kinematic diagram used in order to obtain the dynamic model presented in [33].

Table 1. Robot arm servo actuators

Joint	Model	Max. Torque [Nm]	Resolution [cpr]
1. Base	DM-1050	50	1,024,000
2. Shoulder	DM-1150A	150	1,024,000
3. Elbow	DM-1015B	15	1,024,000
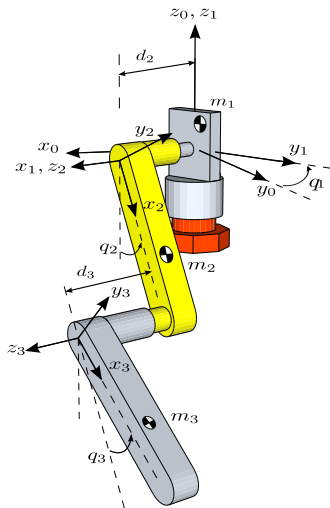
Fig. 3. Kinematic diagram for the experimental robot

(a) Force error of the linear proportional controller
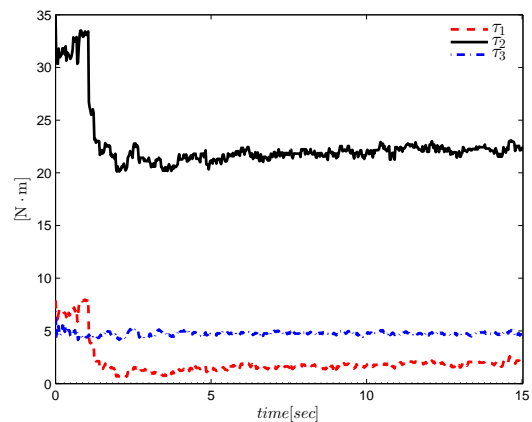
(b) Applied control torques from linear proportional scheme

Fig. 4. Experimental evidence for the linear proportional controller structure

In order to show the performance of the aforementioned controllers, an interaction maneuver is performed. The experiment consists of placing the robot at an initial position, where the third link is normal to a planar wall. Once in this position, the tool attached to the force sensor is very close to the wall, allowing a slight touch. These are the initial conditions of the force-regulation experiment, which is depicted in Figure 2. The desired forces for all the control schemes were:

$$\boldsymbol{f}_d = \begin{bmatrix} f_{xd} \\ f_{yd} \\ f_{zd} \end{bmatrix} = \begin{bmatrix} 0.1 \\ 4.0 \\ 0.1 \end{bmatrix} \text{N} \qquad (37)$$

while the gain matrices for each scheme are described in Table 2.

Now, the results for the different study cases, are presented. For each controller, the force error and the torques applied to the joints, are presented. The linear proportional controller results are depicted in Figures 4(a) and 4(b); the first figure shows the evolution of force error between the reference and the actual force measured with the force/torque sensor, while the second figure shows the applied control torques for all joints.

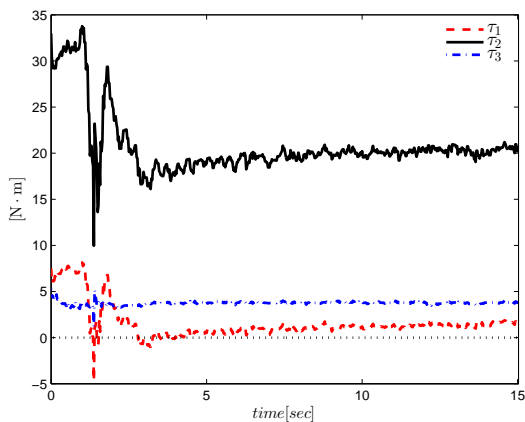*Table 2. Gain matrices for the force regulators*

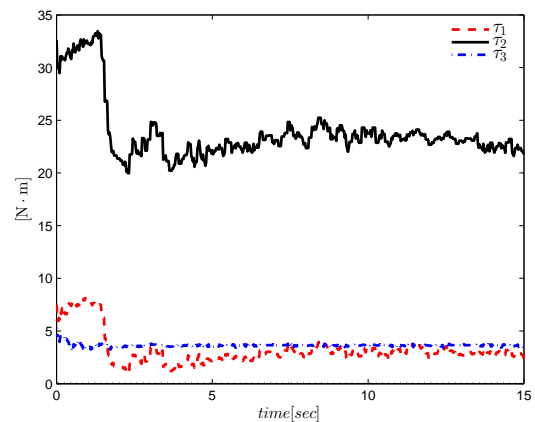| Regulator	K_{pf}	K_v
Linear	diag $(5.0, 10.0, 5.0)$	diag $(150.0, 400.0, 150.0)$
atan	diag $(5.0, 30.0, 5.0)$	diag $(150.0, 400.0, 150.0)$
RSR	diag $(5.0, 39.0, 5.0)$	diag $(150.0, 400.0, 150.0)$
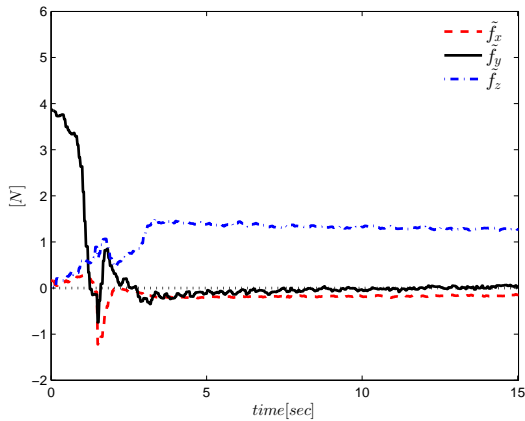
(a) Force error of the atan proportional controller
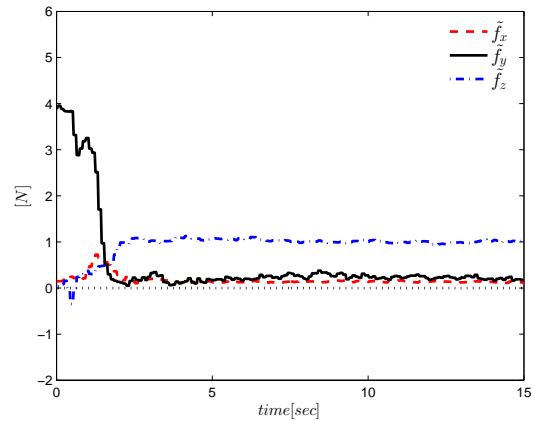
(a) Force error of the RSR proportional controller

(b) Applied control torques from atan proportional scheme

(b) Applied control torques from RSR proportional scheme

Fig. 5. Experimental evidence for the atan proportional controller structure

Fig. 6. Experimental evidence for the RSR proportional controller structure

There exist components of the force error that do not achieve a zero value; the main reason is that the experimental robot lacks a spherical wrist. It is a well-known fact that such a wrist is useful for manipulating the orientation of the end-effector. Figure 4(b) shows that the applied torques are within the range of operation.

Figure 5(a) shows the evolution of the error between the reference and the actual applied force, by using the atan controller, while Figure 5(b) shows the applied con-

trol torques for all joints, using the atan controller. These torques lie within the range of operation.

Lastly, the results corresponding to the RSR controller are presented in the Figure 6(a) for the evolution of error between the reference and the actual applied forces. The applied control torques on the joints can be observed in Figure 6(b), which are, again, within the range of operation.

It is important to notice, as mentioned before, that the experimental robot lacks a spherical wrist, hence, once interaction with the environment exists, the orientation of the end-effector is not controllable. The pose evolves naturally with the robot motion. This particular condition of our experimental robot is the reason why a few components of the force error, do not achieve a zero value. Furthermore, there exist friction forces in the interaction with environment, that have not been modeled in the proposed control scheme.

A method used to evaluate and compare the performance of different regulators consists of using a scalar measure. Since the error between a commanded constant reference and the actual applied force, is a continuous signal with respect to time, the norm $\mathcal{L}_2$ is used to quantize and select the scheme with the best performance. The norm $\mathcal{L}_2$ is given by the following expression,

$$\mathcal{L}_2\{\tilde{\boldsymbol{f}}\} = \sqrt{\frac{1}{t} \int_0^t ||\tilde{\boldsymbol{f}}||^2 \, dt} \tag{38}$$
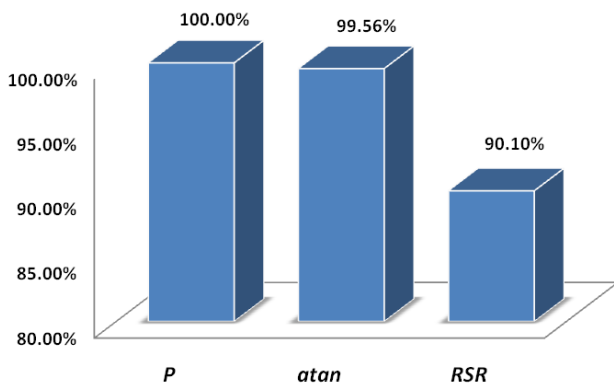

Fig. 7. Normalized norm $\mathcal{L}_2$ of errors

Figure (7) shows the results of the performance, by using the norm $\mathcal{L}_2$ to quantize the error in scalar form. The obtained values are normalized with respect to the largest value, and are presented in percent scale.

The normalized index of error shows that the RSR scheme presents less error as compared to the linear proportional scheme and the atan force regulator, while the

linear proportional scheme presents more error than the rest of the schemes.

6   CONCLUSION

In this paper, a contribution consisting of a new family of explicit force regulators, has been presented. As part of the regulators family, three members have been presented, among them, two newly proposed controllers: atan and RSR proportional control structures. Their performance was compared with the performance of the linear proportional structure, which is widely cited in robotics literature. The new family of explicit force regulators is supported by a stability analysis in Lyapunov sense; it was found that the equilibrium point of the closed-loop system is locally, asymptotically stable in Lyapunov sense.

Experimental results obtained by using a three-degree-of-freedom, direct drive robot, are presented. A six-axis, force/torque sensor ATI FT Gamma SI-130-10, is mounted at the end-effector of the robot manipulator. The experimental evidence shows that the controller with the best performance is the RSR structure, followed by the atan controller, while the linear structure scheme presented the poorest performance.

APPENDIX A   A MATHEMATICAL PROOF OF RELEVANT PROPERTIES

The Cartesian dynamic model has some useful properties for stability analysis of robot controllers. In this Section, an alternative proof for these properties, which are widely cited in the literature of Cartesian robot control, are presented. Specifically, we present the mathematical development for Property 6, Property 7 and Property 8. For validity purposes of the Cartesian dynamic model, it is assumed that the Jacobian matrix is full rank.

Property 6 and Property 7

It is a well known fact that the inertia matrix $M(\boldsymbol{q})$ has the property of being symmetric and positive definite [34]; it follows that

$$\begin{aligned} M_\chi^T &= \left[J^{-T}(\boldsymbol{q})M(\boldsymbol{q})J^{-1}(\boldsymbol{q})\right]^T \\ &= J^{-T}(\boldsymbol{q})M(\boldsymbol{q})^T J^{-1}(\boldsymbol{q}) \\ &= J^{-T}(\boldsymbol{q})M(\boldsymbol{q})J^{-1}(\boldsymbol{q}) \\ &= M_\chi \end{aligned} \tag{39}$$

Taking into account that M_χ is a consistent transformation of $M(\boldsymbol{q})$, then M_χ preserves positive definiteness of $M(\boldsymbol{q})$. Therefore, the Cartesian inertia matrix M_χ is symmetric and positive definite. Property 7 follows immediately from Property 6 and its proof is trivial.

Property 8

First, it is necessary to prove that $\dot{M}_\chi = C_\chi + C_\chi^T$ is valid. With this objective consider $\frac{d}{dt} M_\chi = \dot{M}_\chi$ as follows,

$$
\begin{aligned}
\dot{M}_\chi &= \frac{d}{dt} \left[J^{-T}(\boldsymbol{q}) M(\boldsymbol{q}) J^{-1}(\boldsymbol{q}) \right] \\
&= \left[\frac{d}{dt} J^{-T}(\boldsymbol{q}) \right] M(\boldsymbol{q}) J^{-1}(\boldsymbol{q}) + J^{-T}(\boldsymbol{q}) \dot{M}(\boldsymbol{q}) J^{-1}(\boldsymbol{q}) \\
&\quad + J^{-T}(\boldsymbol{q}) M(\boldsymbol{q}) \left[\frac{d}{dt} J^{-1}(\boldsymbol{q}) \right]
\end{aligned}
\tag{40}
$$

with the purpose of simplifying the above expression, consider $J(\boldsymbol{q}) J^{-1}(\boldsymbol{q}) = I_n$; by differentiating with respect to time and solving for $\frac{d}{dt} J^{-1}(\boldsymbol{q})$, we obtain,

$$
\frac{d}{dt} J^{-1}(\boldsymbol{q}) = -J^{-1}(\boldsymbol{q}) \dot{J}(\boldsymbol{q}) J^{-1}(\boldsymbol{q})
\tag{41}
$$

Also, in a similar fashion, considering $J^T(\boldsymbol{q}) J^{-T}(\boldsymbol{q}) = I_n$ and differentiating with respect to time and solving for $\frac{d}{dt} J^{-T}(\boldsymbol{q})$, we obtain

$$
\frac{d}{dt} J^{-T}(\boldsymbol{q}) = -J^{-T}(\boldsymbol{q}) \left[\frac{d}{dt} J^T(\boldsymbol{q}) \right] J^{-T}(\boldsymbol{q})
\tag{42}
$$

Hence, by substituting (41) and (42) into (40), matrix $\dot{M}_\chi$ takes the following form,

$$
\begin{aligned}
\dot{M}_\chi &= -J^{-T}(\boldsymbol{q}) \left[\frac{d}{dt} J^T(\boldsymbol{q}) \right] M_\chi + J^{-T}(\boldsymbol{q}) \dot{M}(\boldsymbol{q}) J^{-1}(\boldsymbol{q}) \\
&\quad - M_\chi \dot{J}(\boldsymbol{q}) J^{-1}(\boldsymbol{q})
\end{aligned}
\tag{43}
$$

On the other hand,

$$
\begin{aligned}
C_\chi + C_\chi^T &= J^{-T}(\boldsymbol{q}) C(\boldsymbol{q}, \dot{\boldsymbol{q}}) J^{-1}(\boldsymbol{q}) - M_\chi \dot{J}(\boldsymbol{q}) J^{-1}(\boldsymbol{q}) \\
&\quad + J^{-T}(\boldsymbol{q}) C^T(\boldsymbol{q}, \dot{\boldsymbol{q}}) J^{-1}(\boldsymbol{q}) - J^{-T}(\boldsymbol{q}) \left[\frac{d}{dt} J^T(\boldsymbol{q}) \right] M_\chi^T \\
&= -J^{-T}(\boldsymbol{q}) \left[\frac{d}{dt} J^T(\boldsymbol{q}) \right] M_\chi + J^{-T}(\boldsymbol{q}) \dot{M}(\boldsymbol{q}) J^{-1}(\boldsymbol{q}) \\
&\quad - M_\chi \dot{J}(\boldsymbol{q}) J^{-1}(\boldsymbol{q})
\end{aligned}
\tag{44}
$$

where the Property 6 for M_χ and the widely known property [34] $\dot{M}(\boldsymbol{q}) = C(\boldsymbol{q}, \dot{\boldsymbol{q}}) + C^T(\boldsymbol{q}, \dot{\boldsymbol{q}})$ were used in above expression.

By comparing expressions (43) and (44), we conclude that

$$
\dot{M}_\chi = C_\chi + C_\chi^T
\tag{45}
$$

Also it is needed to prove that $C_\chi^T - C_\chi = -\left[C_\chi^T - C_\chi \right]^T$ is a valid expression. With this purpose,

consider the following expression,

$$
\begin{aligned}
C_\chi^T - C_\chi &= \\
&\quad J^{-T}(\boldsymbol{q}) C^T(\boldsymbol{q}, \dot{\boldsymbol{q}}) J^{-1}(\boldsymbol{q}) - J^{-T}(\boldsymbol{q}) \left[\frac{d}{dt} J^T(\boldsymbol{q}) \right] M_\chi^T \\
&\quad - J^{-T}(\boldsymbol{q}) C(\boldsymbol{q}, \dot{\boldsymbol{q}}) J^{-1}(\boldsymbol{q}) + M_\chi \dot{J}(\boldsymbol{q}) J^{-1}(\boldsymbol{q})
\end{aligned}
\tag{46}
$$

On the other hand,

$$
\begin{aligned}
-\left[C_\chi^T - C_\chi \right]^T &= \\
&\quad - \left[J^{-T}(\boldsymbol{q}) C^T(\boldsymbol{q}, \dot{\boldsymbol{q}}) J^{-1}(\boldsymbol{q}) - J^{-T}(\boldsymbol{q}) \left[\frac{d}{dt} J^T(\boldsymbol{q}) \right] M_\chi^T \right. \\
&\quad \left. - J^{-T}(\boldsymbol{q}) C(\boldsymbol{q}, \dot{\boldsymbol{q}}) J^{-1}(\boldsymbol{q}) + M_\chi \dot{J}(\boldsymbol{q}) J^{-1}(\boldsymbol{q}) \right]^T \\
&= -J^{-T}(\boldsymbol{q}) C(\boldsymbol{q}, \dot{\boldsymbol{q}}) J^{-1}(\boldsymbol{q}) + M_\chi \dot{J}(\boldsymbol{q}) J^{-1}(\boldsymbol{q}) \\
&\quad + J^{-T}(\boldsymbol{q}) C^T(\boldsymbol{q}, \dot{\boldsymbol{q}}) J^{-1}(\boldsymbol{q}) \\
&\quad - J^{-T}(\boldsymbol{q}) \left[\frac{d}{dt} J^T(\boldsymbol{q}) \right] M_\chi^T
\end{aligned}
\tag{47}
$$

By comparing expressions (46) and (47), we conclude that

$$
C_\chi^T - C_\chi = -\left[C_\chi^T - C_\chi \right]^T
\tag{48}
$$

Therefore, by using (45) and (48), we obtain

$$
\begin{aligned}
\frac{1}{2} \dot{\boldsymbol{x}}^T \left[\dot{M}_\chi - 2C_\chi \right] \dot{\boldsymbol{x}} &= \frac{1}{2} \dot{\boldsymbol{x}}^T \left[C_\chi + C_\chi^T - 2C_\chi \right] \dot{\boldsymbol{x}} \\
&= \frac{1}{2} \dot{\boldsymbol{x}}^T \left[C_\chi^T - C_\chi \right] \dot{\boldsymbol{x}} \\
&= -\frac{1}{2} \dot{\boldsymbol{x}}^T \left[C_\chi^T - C_\chi \right]^T \dot{\boldsymbol{x}} \\
&= 0
\end{aligned}
$$

Therefore, matrix $\dot{M}_\chi - 2C_\chi$ is skew-symmetric.

ACKNOWLEDGMENT

REFERENCES

[1] B. Siciliano and L. Villani, *Robot Force Control.* Norwell, MA, USA: Kluwer Academic Publishers, 1st ed., 2000.

[2] N. Hogan, "Impedance control - An approach to manipulation. I - Theory. II - Implementation. III - Applications," *ASME Transactions Journal of Dynamic Systems and Measurement Control B*, vol. 107, pp. 1–24, mar 1985.

[3] S. Eppinger and W. Seering, "Introduction to dynamic models for robot force control," *Control Systems Magazine, IEEE*, vol. 7, pp. 48 –52, april 1987.

[4] D. E. Whitney, "Historical perspective and state of the art in robot force control," *International Journal of Robotic Research*, vol. 6, pp. 3–14, mar 1987.

[5] J. De Schutter, H. Bruyninckx, W. H. Zhu, and M. W. Spong, "Force control: a bird's eye view," in *Proceedings of IEEE CSS/RAS International Workshop on Control Problems in Robotics and Automation: Future Directions*, (San Diego, CA), December 1997.

[6] S. Chiaverini, B. Siciliano, and L. Villani, "A survey of robot interaction control schemes with experimental comparison," *Mechatronics, IEEE/ASME Transactions on*, vol. 4, pp. 273 –285, sep 1999.

[7] F. Caccavale, C. Natale, B. Siciliano, and L. Villani, "Integration for the next generation: embedding force control into industrial robots," *Robotics Automation Magazine, IEEE*, vol. 12, pp. 53 – 64, sept. 2005.

[8] J. K. Salisbury, "Active stiffness control of a manipulator in cartesian coordinates," in *Decision and Control including the Symposium on Adaptive Processes, 1980 19th IEEE Conference on*, vol. 19, pp. 95 –100, dec. 1980.

[9] S. R. Oh, H. C. Kim, I. H. Suh, B. J. You, and C. W. Lee, "A compliance control strategy for robot manipulators using a self-controlled stiffness function," in *Intelligent Robots and Systems 95. 'Human Robot Interaction and Cooperative Robots', Proceedings. 1995 IEEE/RSJ International Conference on*, vol. 3, pp. 179 –184 vol.3, aug 1995.

[10] B. H. Kim, N. Y. Chong, S. R. Oh, I. H. Suh, and Y. J. Cho, "Intelligent compliance control for robot manipulators using adaptive stiffness characteristics," in *Robotics and Automation, 1999. Proceedings. 1999 IEEE International Conference on*, vol. 3, pp. 2134 –2139 vol.3, 1999.

[11] N. Tischler and A. Goldenberg, "Stiffness control for geared manipulators," in *Robotics and Automation, 2001. Proceedings 2001 ICRA. IEEE International Conference on*, vol. 3, pp. 3042 – 3046 vol.3, 2001.

[12] H. Mehdi and O. Boubaker, "Stiffness and Impedance Control Using Lyapunov Theory for Robot-Aided Rehabilitation," *International Journal of Social Robotics*, pp. 1–13, 2011.

[13] H. Kazerooni, T. Sheridan, and P. Houpt, "Robust compliant motion for manipulators, part I: The fundamental concepts of compliant motion," *Robotics and Automation, IEEE Journal of*, vol. 2, pp. 83 – 92, jun 1986.

[14] M. Mendoza-Gutiérrez, F. Reyes, I. Bonilla-Gutiérrez, and E. J. González-Galván, "Proportional-derivative impedance control of robot manipulators for interaction tasks," *Proceedings of the Institution of Mechanical Engineers, Part I: Journal of Systems and Control Engineering*, vol. 225, no. 3, pp. 315–329, 2011.

[15] I. Bonilla-Gutiérrez, F. Reyes, M. Mendoza-Gutiérrez, and E. J. González-Galván, "A Dynamic-compensation Approach to Impedance Control of Robot Manipulators," *Journal of Intelligent & Robotic Systems*, vol. 63, pp. 51–73, 2011.

[16] R. Volpe and P. Khosla, "A theoretical and experimental investigation of explicit force control strategies for manipulators," *Automatic Control, IEEE Transactions on*, vol. 38, pp. 1634 –1650, nov 1993.

[17] S. Singh and D. Popa, "An analysis of some fundamental problems in adaptive control of force and impedance behavior: theory and experiments," *Robotics and Automation, IEEE Transactions on*, vol. 11, pp. 912 –921, dec 1995.

[18] B. Siciliano, L. Sciavicco, L. Villani, and G. Oriolo, *Robotics: Modelling, Planning and Control*. Springer Publishing Company, Incorporated, 2010.

[19] M. H. Raibert and J. J. Craig, "Hybrid Position/Force Control of Manipulators," *Journal of Dynamic Systems, Measurement, and Control*, vol. 103, no. 2, pp. 126–133, 1981.

[20] T. Yoshikawa, T. Sugie, and M. Tanaka, "Dynamic hybrid position/force control of robot manipulators-controller design and experiment," *Robotics and Automation, IEEE Journal of*, vol. 4, pp. 699 –705, dec 1988.

[21] R. Lozano and B. Brogliato, "Adaptive hybrid force-position control for redundant manipulators ," *Automatic Control, IEEE Transactions on*, vol. 37, pp. 1501 –1505, oct 1992.

[22] D. Jeon and M. Tomizuka, "Learning hybrid force and position control of robot manipulators ," *Robotics and Automation, IEEE Transactions on*, vol. 9, pp. 423 –431, aug 1993.

[23] G. Ferretti, G. Magnani, and P. Rocco, "Toward the implementation of hybrid position/force control in industrial robots," *Robotics and Automation, IEEE Transactions on*, vol. 13, pp. 838 –845, dec 1997.

[24] S. Chiaverini and L. Sciavicco, "The parallel approach to force/position control of robotic manipulators," *Robotics and Automation, IEEE Transactions on*, vol. 9, pp. 361 – 373, aug 1993.

[25] Q. H. Xia, S. Y. Lim, M. Ang, and T. M. Lim, "Parallel force and motion control using adaptive observer-controller," in *Systems, Man and Cybernetics, 2008. SMC 2008. IEEE International Conference on*, pp. 3143 –3149, oct. 2008.

[26] Alexandre Denève and Saïd Moughamir and Lissan Afilal and Janan Zaytoon, "Control system design of a 3-dof upper limbs rehabilitation robot," *Computer Methods and Programs in Biomedicine*, vol. 89, no. 2, pp. 202 – 214, 2008.

[27] R. Anderson and M. Spong, "Hybrid impedance control of robotic manipulators," *Robotics and Automation, IEEE Journal of*, vol. 4, pp. 549 –556, oct 1988.

[28] R. Carelli and R. Kelly, "An adaptive impedance/force controller for robot manipulators," *Automatic Control, IEEE Transactions on*, vol. 36, pp. 967–971, aug 1991.

[29] M. Hosseinzadeh, P. Aghabalaie, H. Talebi, and M. Shafie, "Adaptive Hybrid Impedance Control of robotic manipulators," in *IECON 2010 - 36th Annual Conference on IEEE Industrial Electronics Society*, pp. 1442–1446, nov. 2010.

[30] A. Loria and R. Ortega, "Force/position regulation for robot manipulators with unmeasurable velocities and uncertain gravity," *Automatica*, vol. 32, pp. 939–943, jul. 1996.

[31] M. Takegaki and S. Arimoto, "A New Feedback Method for Dynamic Control of Manipulators," *Journal of Dynamic Systems, Measurement, and Control*, vol. 103, no. 2, pp. 119–125, 1981.

[32] M. Vidyasagar, *Nonlinear Systems Analysis*. Prentice Hall, 1993.

[33] C. Chávez-Olivares, F. Reyes-Cortés, E. González-Galván, M. Mendoza-Gutiérrez, and I. Bonilla-Gutiérrez, "Experimental evaluation of parameter identification schemes on an anthropomorphic direct drive robot," *International Journal of Advanced Robotic Systems*, vol. 9:203, 2012.

[34] R. Kelly, V. Santibáñez, and A. Loría, *Control of Robot Manipulators in Joint Space*. Springer, 2005.

C. Chávez-Olivares was born in Aguascalientes, Mexico on January 12, 1983. He received the B.S. degree in electronics engineering from the Universidad Autónoma de Aguascalientes, Aguascalientes, México, in 2006, and the M.Eng. and Ph.D. degrees in electrical engineering from the Universidad Autónoma de San Luis Potosí, México, in 2009 and 2014, respectively. In 2006, he joined the Department of Electronic Systems, Universidad Autónoma de Aguascalientes, as an Assistant Professor. In 2014, he joined the Departament of Catedras CONACyT and Instituto Tecnológico de Aguascalientes, Aguascalientes, México, where is currently a Professor and Researcher. His research interests include vision systems, modeling, identification, and control of robot manipulators.

F. Reyes-Cortés was born in Puebla, Mexico, on March 7, 1962. He received the B.S. degree in electronics engineering from the Benemérita Universidad Autónoma de Puebla, Puebla, México, in 1984, the M.S. degree from the Instituto Nacional de Astrofísica, Óptica y Electrónica, Puebla, in 1989, and the Ph.D. degree in electronics from the Centro de Investigación Científica y de Educación Superior de Ensenada (CICESE), Ensenada, Mexico, in 1997. In 1980, he joined the Benemérita Universidad Autónoma de Puebla, where he is currently a Professor and Researcher. He has published four books and more than 250 scientific papers in national and international conferences and journals. His research interests include the fields on control of robot manipulators with special emphasis on practical applications.

E. González-Galván was born in Mexico City on April 24, 1965. He received the Bachelor's and Master's degrees from the Universidad de Guanajuato, Guanajuato, Mexico, in 1990 and 1991, respectively, and the Ph.D. degree from the University of Notre Dame, Notre Dame, IN, in 1995, all in mechanical engineering. From 1991 to 1996, he was a Fulbright scholar with the University of Notre Dame, where he became a Postdoctoral Fellow in 1996. From 2007 to 2008, he was a Visiting Scholar with the Massachusetts Institute of Technology. In 1996, he joined the School of Engineering, Universidad Autónoma de San Luis Potosí, San Luis Potosí, México, where he is currently a Professor and Researcher. Dr. González-Galván was the President of the Mexican Robotics Association from 2003 and 2005.

AUTHORS' ADDRESSES

César Chávez-Olivares
1) Departamento de Ingeniería de Metal-Mecánica,
Instituto Tecnológico de Aguascalientes,
Av. Adolfo López Mateos 1801 Oriente, Fracc. Bona Gens,
Aguascalientes, Ags. 20256 México
2) Departamento de Cátedras CONACyT,
CONACyT,
Insurgentes Sur 1582, Col. Crédito Constructor, Del. Benito Juárez, 03940 México D.F.

Fernando Reyes-Cortés
Grupo de Robótica,
Facultad de Ciencias de la Electrónica,
Benemérita Universidad Autónoma de Puebla,
18 Sur y Av. San Claudio, Ciudad Universitaria, Puebla, Pue., 75570 México

Emilio González-Galván
Centro de Investigación y Estudios de Posgrado,
Facultad de Ingenieréa,
Universidad Autónoma de San Luis Potosí,
Av. Manuel Nava 8, Zona Universitaria, San Luis Potosí, S.L.P. 78290 México